Available online at www.sciencedirect.com

SciVerse ScienceDirect

Procedia Engineering 58 (2013) 320 – 327

Procedia Engineering

www.elsevier.com/locate/procedia

The 12th Hypervelocity Impact Symposium

Large scale Optimal Transportation Meshfree (OTM) Simulations of Hypervelocity Impact

B. Li, L. Perotti, M. Adams, J. Mihaly, A.J. Rosakis, M. Stalzer and Michael Ortiz[a]*

[a]*Graduate Aeronautical Laboratories, California Institute of Technology, Pasadena, CA USA 91125*

Abstract

Large scale three-dimensional numerical simulations of hypervelocity impact of Aluminum alloy 6061-T6 plates by Nylon 6/6 cylindrical projectile have been performed using the Optimal Transportation Meshfree (OTM) method of Li *et al.* [7] along with the seizing contact and variational material point failure algorithm [17, 18]. The dynamic response of the Al6061-T6 plate including phase transition in the high strain rate, high pressure and high temperature regime expected in our numerical analysis is described by the use of a variational thermomechanical coupling constitutive model with SESAME equation of state, rate-dependent J2 plasticity with power law hardening and thermal softening and temperature dependent Newtonian viscosity. A polytropic type of equation of state fit to in-house ReaxFF calculations is employed to model the Nylon 6/6 projectile under extreme conditions. The evaluation of the performance of the numerical model takes the form of a conventional validation analysis. In support of the analysis, we have conducted experiments over a range of plate thicknesses of [0.5, 3.0] mm, a range of impact velocities of [5.0, 7.0]km/s and a range of obliquities of [0, 70]^{o} at Caltech's Small Particle Hypervelocity Range (SPHIR) Facility. Large scale three-dimensional OTM simulations of hypervelocity impact are performed on departmental class systems using a dynamic load balancing MPI/PThreads parallel implementation of the OTM method. We find excellent full field agreement between measured and computed perforation areas, debris cloud and temperature field.

Keywords: optimal transportation meshfree, hypervelocity impact, material point failure, thermomechanical coupling

1. Introduction

It's well known there are many complexities associated with the hypervelocity impact. Experiments may be very expensive and time consuming, and it's possible to obtain very few data by the limitation of current laboratory facilities. Numerical methods, on the other hand, have become very useful and important tools to predict the complex phenomena and look into the details of the entire process. However the accurate simulation of hypervelocity impact is a grand challenge in scientific computing that places exacting demands on physics models, numerical solvers and computing resources. In order to meet these challenges, we develop an Optimal Transportation Meshfree (OTM) method for simulating extremely large deformation and hypervelocity impact problems.

The proposed OTM method is a meshfree updated-lagrangian methodology which combines concepts from Optimal Transportation theory with material-point sampling and local max-ent meshfree approximation, and overcomes the essential difficulties in grid-based numerical methods like Lagrangian and Eulerian finite element method. The rationale behind the approach is as follows. We resort the Benamou-Brenier [3] differential formulation of optimal mass transportation problems

* Corresponding author. Tel.: +1 626 395 8640.
E-mail address: ortiz@aero.caltech.edu

doi:10.1016/j.proeng.2013.05.036

and its connection to the Wasserstein distance [5] to discretize the inertial action in space and time within a strictly variational framework. The resulting discretization may be regarded as the result of restricting the inertial action to mass measures concentrated on material points undergoing piecewise rectilinear motions. The density of such mass measures and the constrained minimization structure of the problem may be expected to confer the discretization robust convergence properties. The optimal transportation variational framework also results in: proper mass matrices and inertia forces in the presence of continuously varying spatial interpolation; geometrically exact mass transport and satisfaction of the continuity equation; and exact linear and angular momentum conservation. Finally, fields requiring differentiation, such as deformation and velocity fields, are interpolated from nodal values using max-ent shape functions. These shape functions are reconstructed continuously from the nodal set and have the key property of possessing a Kronecker-delta property at the boundary, which enables the direct imposition of displacement boundary conditions. An energy-based material-point erosion algorithm is also proposed for simulating fracture and fragmentation phenomena. The convergence of the material-point erosion algorithm to Griffith-fracture solutions is ensured by means of Γ-convergence [9]. Three dimensional OTM simulations with material-point erosion algorithm of impact of metallic plates by spherical particles have been conducted. The accuracy and performance of the method in presence is illustrated in this paper by comparing with the in-house experiments.

Following a brief description of the methodology and the variational material-point failure algorithm in section 2, the thermomechanical coupling framework for the material modeling of the target and projectile is presented in section 3. The main numerical results using the OTM method with the comparison to the in-house experiment results are shown in section 4. In section 5 the main conclusion afforded by the analysis is provided.

2. Methodology

2.1. The Optimal Transportation Meshfree method

We begin by briefly summarizing the OTM method of spatial and temporal discretization. A class of semi-discrete actions that is well-suited to computation is

$$S_d\,(\varphi_1,\dots,\varphi_{N-1}) = \sum_{k=0}^{N-1}\left\{\frac{1}{2}\frac{d_W^2(\rho_k,\rho_{k+1})}{(t_{k+1}-t_k)^2}-\frac{1}{2}[U(\varphi_k)+\,U(\varphi_{k+1})]\right\}(t_{k+1}-t_k) \tag{1}$$

where $\varphi_k\colon B\subset\mathbb{R}^n\ \to\mathbb{R}^n$ is the deformation mapping at time t_k, ρ_k is the corresponding mass density at time t_k,

$$U(\varphi) = \int_B f(\nabla\varphi)\ dx \tag{2}$$

is the free energy of the solid, $f(\nabla\varphi)$ is the local free-energy density per unit volume, and

$$d_W^2(\rho_a,\rho_b) = \ \mathrm{Inf}_{(T:B\to B \text{ and } \rho_a=\rho_b\backslash det(\nabla T))}\ \int |T(x)-\,x|^2\rho_a(x)\,dx \tag{3}$$

is the Wasserstein distance between consecutive densities. The term $\frac{1}{2}d_W^2(\rho_k,\rho_{k+1})(t_{k+1}-t_k)$ in Eq.(1) supplies a measure of the inertial action between times t_k and t_{k+1}. We also note that in writing Eq.(1) we have restricted attention to elastic behavior and unforced systems for simplicity. Extensions accounting for forcing, e.g., in the form of body forces, boundary traction, and extensions to inelasticity may be found in [7].

In order to obtain a fully discrete action for computations, we begin by approximating the usual Lebesgue measure $\mathcal{L}$ of the volume at t_k by discrete measures of the form

$$\mathcal{L}_{k,h} = \sum_{p=1}^{M} v_{p,k}\delta(x-x_{p,k}) \tag{4}$$

concentrated at *material points* $x_{p,k}$, each of which is assigned a discrete volume $v_{p,k}$. The discretization of the mass densities $\rho_{k,h}$ may be achieved simply by identifying the discrete mass distributions as measures that are absolutely continuous with respect to the discrete volume measure $\mathcal{L}_{k,h}$, with Radon-Nykodim density $\rho_{h,k}$, namely,

$$\rho_{h,k}(\mathrm{x}) = \sum_{\mathrm{p}=1}^{\mathrm{M}} \rho_{\mathrm{p,k}} \mathrm{v}_{\mathrm{p,k}} \delta\left(\mathrm{x} - \mathrm{x}_{\mathrm{p,k}}\right) \tag{5}$$

The quantity $m_p = \rho_{p,k}\, v_{p,k}$ may be regarded as the mass carried by material point p. Li *et al.* [7] have shown that the constancy of the material point masses m_p is indeed equivalent to the weak satisfaction of the continuity equation. To complete the spatial discretization, we approximate the incremental deformation mapping as

$$\varphi_{h,k\to k+1}(x) = \sum_{a=1}^{\mathbb{N}} x_{a,k+1} N_{a,k}(x) \tag{6}$$

where $\{x_{a,k+1}, a = 1, \dots, \mathbb{N}\}$ is an array of nodal coordinates at time t_{k+1} and $N_{a,k}(x)$ are conforming shape functions defined over the configuration at time t_k. In calculations, we specifically use max-ent shape functions [1] computed from the array $\{x_{a,k+1}, a = 1, \dots, \mathbb{N}\}$ of nodal coordinates at time t_{k+1}. Since max-ent shape functions are strongly localized, the interpolation at a material point $x_{p,k}$ depends solely on the nodes contained in a small *local neighborhood* of the material point, Figure 1. In calculations, the local neighborhoods are continuously updated using range searches [4] to account for the relative motion between material points and nodes.

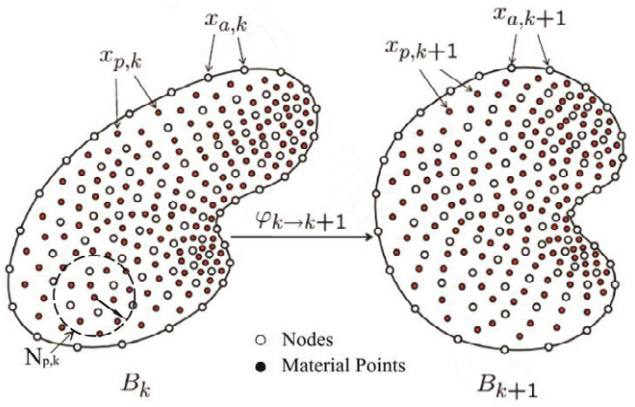

Figure 1 The optimal transportation meshfree methodology.

Inserting these approximations into Eq. (1) we obtain the fully-discrete action

$$S_d\left(\varphi_{h,1}, \dots, \varphi_{h,N-1}\right) = \sum_{\mathrm{k}=0}^{\mathrm{N}-1} \left\{ \frac{\mathrm{m_p}}{2} \frac{\left|\mathrm{x_{p,k+1}} - \mathrm{x_{p,k}}\right|^2}{(\mathrm{t_{k+1}} - \mathrm{t_k})^2} - \frac{\mathrm{v_{p,k}}}{2} \left[\mathrm{f}\left(\nabla \varphi_{\mathrm{h,k}}\left(\mathrm{x_{p,k}}\right)\right) + \mathrm{f}\left(\nabla \varphi_{\mathrm{h,k+1}}\left(\mathrm{x_{p,k+1}}\right)\right) \right] \right\} (\mathrm{t_{k+1}} - \mathrm{t_k}) \tag{7}$$

where we again consider the unforced elastic case for simplicity. The discrete trajectories now follow from the discrete Hamilton's principle $\delta S_h = 0$ of stationary action.

We see from Figure 1 that the OTM scheme can be solved forward explicitly. This forward solution has the usual structure of explicit time-integration and updated-Lagrangian schemes. In particular, all the finite kinematics of the motion, including the mass density and volume updates, are geometrically exact. In addition, the continuous reconstruction of the local material-point neighborhoods and shape functions has the effect of automatically reconnecting the material points and the nodal set, at no cost of remapping the local states carried by the material points. This property of the method is particularly convenient for inelastic materials whose local material state often includes additional internal variable information. A particularly convenient feature of OTM, which is common to other material-point based methods [2], is that *seizing contact* is automatically accounted for. This is so because of the cancelation of linear momentum that naturally occurs when colliding nodes come within the local neighborhoods of material points.

Nevertheless considerable savings on computational time for the OTM method will be realized with a successful utilization of parallel computers. The OTM method including the dynamic contact algorithm is essentially a Single Instruction Multiple Data (SIMD) parallel approach as most of the operations are performed at every material point locally. Therefore a hybrid MPI/PThreads implementation of the OTM method at the levels of distributed memory and shared memory systems is straight forward. Similar to explicit finite element codes, the parallelization is made with regard to the determination of nodal forces in parallel. Domain decomposition is performed by distributing material points across processors and nodal information is synchronized using a dynamically reconstructed communication map between distributed processors. The parallel OTM algorithm resulting from the preceding scheme is listed in Algorithm 1.

For Processor $\mathbb{P}^I, I = 1, \dots, P$:
REQUIRE: Initial and final times for time step, t_k and t_{k+1};
REQUIRE: Initial nodal coordinates, $\mathcal{S}_k^I = \{x_{a,k} \in \mathbb{P}^I, a = 1, \dots, N\}$;
REQUIRE: Initial material-point coordinates, $\{x_{p,k}^I, p = 1, \dots, M\}$;
REQUIRE: Initial neighborhood of material points, $NH(x_{p,k}) = \{x_{a,k}, |x_{a,k} - x_{p,k}^I| \le d(x_{p,k})\}$, where $d(x_{p,k})$ is the dynamic support size of material point $x_{p,k}^I$ and condition $\cup_p NH(x_{p,k}) \subseteq \mathcal{S}_k^I$ must be satisfied;
REQUIRE: Initial shape functions $\{N_{a,k}(x_{p,k}^I), a \in NH(x_{p,k}), p = 1, \dots, M\}$;
REQUIRE: Ibid gradients $\{\nabla N_{a,k}(x_{p,k}^I), a \in NH(x_{p,k}), p = 1, \dots, M\}$;
REQUIRE: Initial deformation gradients $\{F_{p,k}, p = 1, \dots, M\}$;
REQUIRE: Initial material state at all material points on $\mathbb{P}^I$;
REQUIRE: Initial communication map $\mathbb{C}_k$.
1: Compute mass matrix M_k^I, nodal forces f_k^I for all nodes in $\mathcal{S}_k^I$ locally on $\mathbb{P}^I$;
2: Asynchronous send and receive information of shared nodes based on $\mathbb{C}_k$using MPI;
3: Correct mass matrix, nodal forces for nodes in $\mathcal{S}_k^I$, compute total nodal accelerations $a_k^I = (M_k^I)^{-1} f_k^I$;
4: Update nodal coordinates: $x_{k+1}^I = x_k^I + (t_{k+1} - t_k)(v_k^I + \frac{1}{2}(t_{k+1} - t_{k-1})a_K^I)$;
5: Update nodal velocities: $v_{k+1}^I = (x_{k+1}^I - x_k^I)/(t_{k+1} - t_k)$;
6: Update material point coordinates: $x_{p,k+1}^I = \varphi_{k\to k+1}(x_{p,k}^I), p = 1, \dots, M$;
7: Update deformation gradients: $F_{p,k+1} = \nabla\varphi_{k\to k+1}(x_{p,k}^I)F_{p,k}, p = 1, \dots, M$;
8: Effect constitutive updates at material points;
9: Update local material point neighborhood $NH(x_{p,k+1}), p = 1, \dots, M$;
10: Compute shape functions and their derivatives: $\{N_{a,k}(x_{p,k+1}^I), \nabla N_{a,k}(x_{p,k+1}^I), a \in NH(x_{p,k+1}), p = 1, \dots, M\}$;
11: Update communication map $\mathbb{C}_{k+1}$.

Algorithm 1 Parallel Optimal Transportation Meshfree (POTM) scheme

2.2. The Material-Point failure algorithm

Finally, we briefly outline the material-point erosion algorithm proposed to simulate the fracture and fragmentation phenomena in hypervelocity impact calculations. Within the context of OTM calculations, fracture can be modeled simply by failing material points according to an energy-release criterion [17, 18]. Following Fraternali *et al*. [9] we compute the energy-release rate attendant to the failure of material point p as

$$G_{p,k+1} = \frac{Ch_p}{\sum_{x_{q,k+1} \in B_\epsilon(x_{p,k+1})} m_q} \sum_{x_{q,k+1} \in B_\epsilon(x_{p,k+1})} m_q f_k(F_{q,k+1}) \tag{8}$$

where $B_\epsilon(x_{p,k+1})$ is the ball of radius ϵ centered at $x_{p,k+1}$. The radius ϵ defines a length scale intermediate between the discretization size and the macroscopic size of the bodies. The material point is failed when

$$G_{p,k+1} \ge G_c \tag{9}$$

where G_c is a critical energy release rate that measures the material-specific energy required to create a fracture surface of unit area. For linear elasticity, Fraternali *et al.* have shown that criterion (8) and (9) result in approximations that converge to Griffith fracture in the limit of an infinitely fine discretization.

3. Constitutive Model

During hypervelocity impacts, materials are subjected to extremely large deformations rate, high pressures and temperature. In order to properly describe the material response of the target aluminum plate, we develop a material model in a variational thermomechanical coupling framework. This framework accounts for thermo-viscoplasticity, temperature dependent viscosity, employs equations of state (EoS) to describe the volumetric response in the high pressure-temperature regimes, and allows studying the partition of plastic work in stored and dissipated energy in a systematic fashion. We begin with a brief summary of the thermomechanical framework on which we have based our calculations. A detailed description of the constitutive model may be found in [13]. It is essential for the purpose of the optimal transportation structure that the resulting stress update algorithm derives from an incremental potential, or energy density, so that the incremental displacements are governed by a minimum principle. To this end, we adopt a standard constitutive update algorithm that takes the form of minimization of a local incremental energy as shown in [8, 12], especially the incremental energy density per unit volume is defined as

$$f\left(F_{k+1}; F_k, F_k^p, \bar{\epsilon}_k^p, T_k\right) = \sup_{T_{k+1}} \mathcal{W}_{k+1}(F_{k+1}, T_{k+1}; F_k, F_k^p, \bar{\epsilon}_k^p, T_k) \tag{10}$$

and

$$\begin{aligned} \mathcal{W}_{k+1}\left(F_{k+1}, T_{k+1}; F_k, F_k^p, \bar{\epsilon}_k^p, T_k\right) \equiv \inf_{\mathrm{Z}} \Big\{ & W\left(F_{k+1}, F_{k+1}^p, \bar{\epsilon}_{k+1}^p, T_{k+1}\right) - W_k + \rho_0 \eta_k (T_{k+1} - T_k) \\ & + (\mathrm{t_{k+1}} - \mathrm{t_k}) \left[\Psi^* \left(\frac{T_{k+1}}{T_k} \frac{\Delta \bar{\epsilon}^p}{\Delta t} \right) \right]_{\Delta t} \Big\} + (t_{k+1} - t_k) \left[\Phi^* \left(\frac{T_{k+1}}{T_k} \frac{\Delta F}{\Delta t} \right) \right]_{\Delta t} \end{aligned} \tag{11}$$

where F is the deformation gradient assumed for a multiplicative elastic-plastic finite kinematics [6], i.e., $F = F^e F^p$ with F^e and F^p as the elastic and plastic part of the deformation gradient respectively, W is the free energy density, η is the specific entropy, Z denotes a vector of internal variables such as $\bar{\epsilon}^p$, a scalar internal variable measuring the cumulated plastic strain in a macroscopic plasticity model of the von-Mises type, and the local material state is completed with the absolute temperature T. The last two terms in Eq. (11) denotes some approximation to the average of the dissipation pseudo-potentials $\Psi^*$and Φ^*conjugated to the rate of the local internal processes and the rate of deformation gradient over the time step Δt respectively. An example of consistent approximation is shown in [10].

In materials such as metals, the elastic response and the specific heat are ostensibly independent of the internal processes and the free energy density in Eq. (11) may be decomposed additively as

$$W = W^e\left(FF^{p-1}, T\right) + W^p(F^p, \bar{\epsilon}^p, T) + W^h(T) \tag{12}$$

where the function W^e determines the elastic response of the metal, whereas the function W^p represents the stored energy due to the plastic working and the thermal energy W^h describes the heat storage capacity of the material. In particular, we consider the following free energies in Eq. (12) and dual dissipation psuedo-potential in Eq. (11),

$$\begin{aligned} W^e(F^e, T) &= W^{e,vol}(\theta, T) + G(\theta, T) \parallel e^e \parallel^2 \\ W^p(F^p, \bar{\epsilon}^p, T) &= \omega(T) \frac{l}{l+1} \sigma_y \bar{\epsilon}_0^p \left(1 + \frac{\bar{\epsilon}^p}{\bar{\epsilon}_0^p} \right)^{\frac{l+1}{l}} \\ W^h(T) &= \rho_0 C_0 T \left(1 - \log \frac{T}{T_0} \right) \\ \Psi^* \left(\frac{\Delta \bar{\epsilon}^p}{\Delta t} \right) &= \omega(T) \frac{m}{m+1} \, \sigma_y (\dot{\bar{\epsilon}})_0^p \left(\frac{1}{\Delta t} \frac{\Delta \bar{\epsilon}^p}{(\dot{\bar{\epsilon}})_0^p} \right)^{\frac{m+1}{m}} \end{aligned} \tag{13}$$

where θ is the elastic volumetric deformation and $\omega(T)$ is the thermal softening function defined as

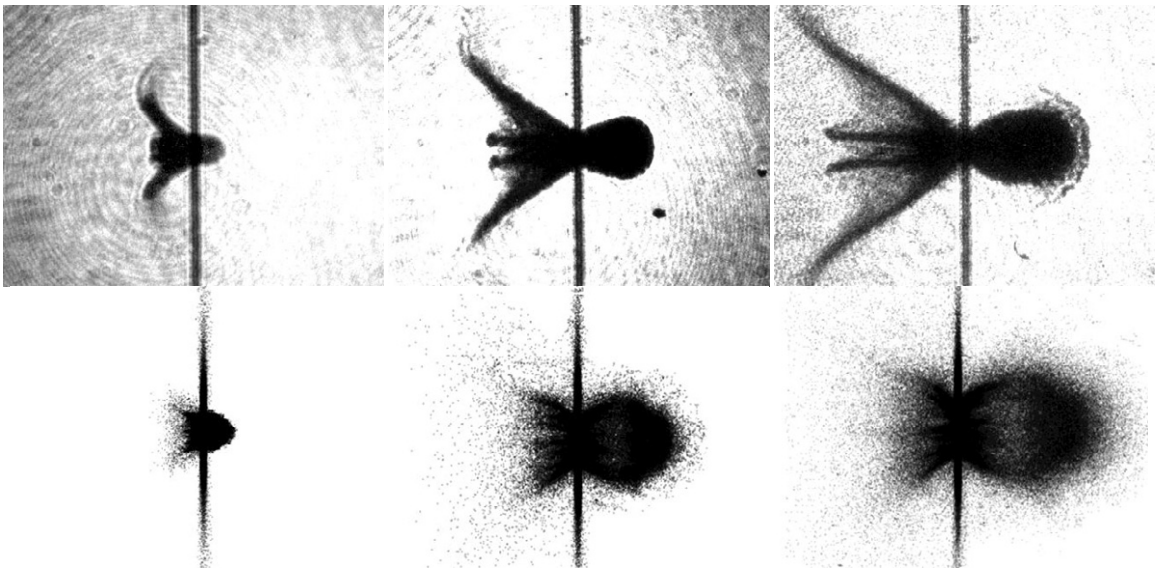

Figure 2 Hypervelocity impact experiment (top) conducted at Caltech's Small Particle Hypervelocity Range Facilities (SPHIR) and OTM simulation (bottom) of 0.5mm thick Al6061-T6 plates by Nylon 6/6 cylindrical projectiles at 5.44 km/s. Shadow graphs captured at $t = 0.5, 3.0$ and$4.7\mu s$

.

$$\omega(T) = \begin{cases} \left(1 - \dfrac{T - T_0}{T_m - T_0}\right)^a & \text{if } T < T_m \\ 0 & \text{otherwise} \end{cases} \tag{14}$$

Finally, the material with Newtonian viscosity can be described by the following expression for the dissipation potential

$$\Phi^*\left(\dot{\mathrm{F}}, \mathrm{T}\right) = \mu(\mathrm{T})\ \mathrm{Det}(\mathrm{F})\ \|\ \mathrm{D}^{\mathrm{dev}}\ \|^2 \tag{15}$$

where $D = sym\left(\dot{F}F^{-1}\right)$ is the rate of deformation tensor and $\mu(T)$ is the viscosity coefficient as a function of absolute temperature. For instance for liquid aluminum, the following equation may be used [15]

$$\mu(T) = \mu_0 \exp\left(-a_1 + \frac{a_2}{T}\right) \tag{16}$$

4. Numerical Results

In order to validate the OTM method with the variational material point failure algorithm and the thermomechanical constitutive model, a series of in-house experiments of Aluminum 6061-T6 plates impact by Nylon 6/6 cylindrical projectiles are performed at Caltech's Small Particle Hypervelocity Range Facilities (SPHIR) [16]. The diameter of the projectile is 1.8mm and length 1.8mm as well. The length and width of the plate is 152mm and thickness is in the range of 0.5 to 3.0mm. The range of investigation covers the impact velocity from 5 to 7km/s and obliquity from 0^o to 70^o. In all calculations the same configurations corresponding to experiments are employed and the constitutive model described in section 3 is used. The material parameters in the thermomechanical coupling framework have been chosen according to the related literatures [11] and computed by in-house ReaxFF molecular dynamics simulations [14] which may be found in [13]. Large scale three dimensional OTM simulations have been carried out in the Shared Heterogeneous Cluster (SHC) of Caltech's Center for Advanced Computing Research (CACR). The SHC configuration consists of 1,156 AMD Opteron cores and an Infiniband connection. Our three-dimensional OTM simulation with the discretization of the order of 10^6 material points takes 12 hours or CPU time to finish $5\mu s$ simulation time using 512 SHC AMD Opteron cores.

Figure 2 shows a typical perforation process for the impact of a 0.5mm Al6061-T6 plate by a nylon 6/6 cylindrical particle at 5.44km/s. A direct comparison of the OTM calculated results against experimental measurements is illustrated through the correlated shadow graphs of the perforation process. The predicted perforation area in our OTM simulation for this configuration is 13.85mm^2 and the measured hole size in experiment is 13.3mm^2. The ability of OTM to simulate extreme conditions of material response, including high pressures, strain rates and temperatures, large inelastic deformations, phase transitions such as melting, transport properties such as viscosity, and failure mechanisms such as fracture and fragmentation, is noteworthy. A very fine simulation with totally 2,042,320 material points and 1,660,470 degrees of freedom is shown in Figure 3 for the demonstration of the robustness and convergence of the OTM method.

5. Conclusion

We have presented an Optimal Transportation Meshfree (OTM) method which enables the prediction of hypervelocity impact. The theoretical basis of the OTM method guarantees the exact conservation of mass, linear and angular momentum. The proposed material point erosion algorithm greatly extends the applicability of the OTM method. The performance and accuracy of the proposed method has been tested by three dimensional hypervelocity impact simulations and in-house experiments. The agreement between numerical and experimental results is excellent.

Acknowledgements

The authors gratefully acknowledge the support of the Department of Energy National Nuclear Security Administration under Award Number DE-FC52-08NA28613 through Caltech's ASC/PSAAP Center for the Predictive Modeling and Simulation of High Energy Density Dynamic Response of Materials.

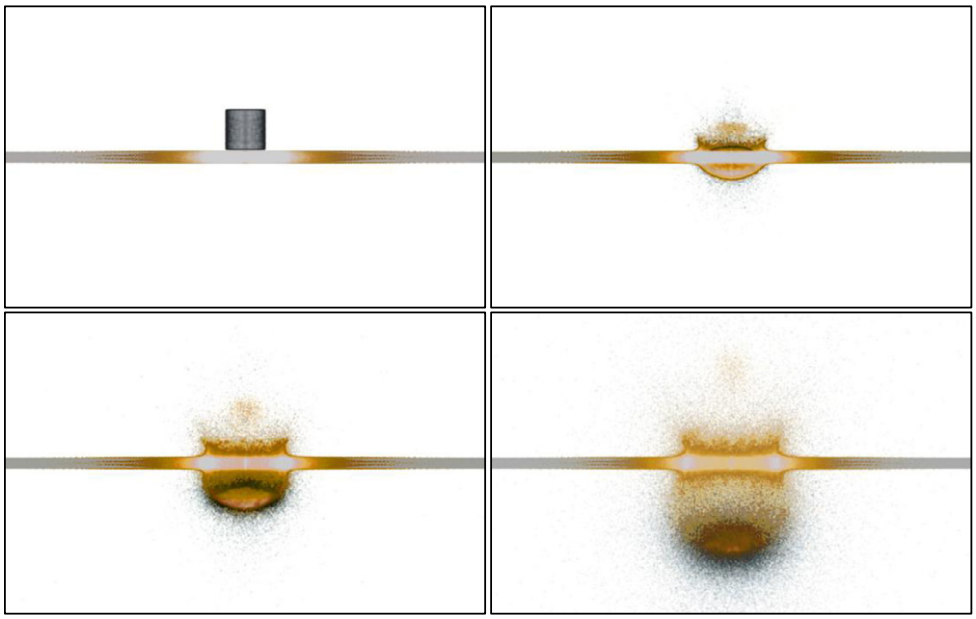

Figure 3 Perforation of 0.5mm thick Aluminum plate at impact velocity 5.2km/s by OTM method. Snapshots at $t = 0, 0.25, 0.5$ and $1.0\ \mu s$

References

[1] M. Arroyo and M. Ortiz, 2006. Local maximum-entropy approximation schemes: A seamless bridge between finite elements and meshfree methods. International Journal for Numerical Methods in Engineering 65, p.2167−2202.
[2] S.G. Bardenhagen, J.U. Brackbill, and D. Sulsky, 2000. The material-point method for granular materials. Computer Methods in Applied Mechanics and Engineering, 187(3−4), p. 529−541.
[3] J. D. Benamou and Y. Brenier,1999. A numerical method for the optimal time-continuous mass transport and related problems. in: Monge-Ampere equation: applications to geometry and optimization. Contemp. Math. 226, p. 1−11.
[4] J. L. Bentley and J. H. Friedman, 1998. Data structures for range searching. Computing Surveys, 11, p. 397−409, 1979.[5] R. Jordan, D. Kinderlehrer, and F. Otto. The variational formulation of the Fokker-Planck equation. SIAM J.Math. Anal., 29, p. 1−17.
[6] E. H. Lee, 1969. Elastic-plastic deformations at finite strains. Journal of Applied Mechanics, 36(1), p. 1−6.
[7] B. Li, F. Habbal, and M. Ortiz, 2010. Optimal transportation meshfree approximation schemes for fluid and plastic flows. International Journal for Numerical Methods in Engineering, 83(12), p. 1541−1579.
[8] M. Ortiz and L. Stainier, 1999. The variational formulation of viscoplastic constitutive updates. Computer Methods in Applied Mechanics and Engineering, 171(3-4), p. 419−444.
[9] B. Schmidt, F. Fraternali, and M. Ortiz, 2009. Eigenfracture: An eigendeformation approach to variational fracture.Multiscale Modeling and Simulation, 7, p. 1237−1266.
[10] L. Stainier, 2011. Consistent incremental approximation of dissipation pseudo-potentials in the variational formulation of thermo-mechanical constitutive updates. Mechanics Research Communications, 38(4), p. 315−319.
[11] S. Yadav, EA Repetto, G. Ravichandran, and M. Ortiz, 2001. A computational study of the influence of thermal softening on ballistic penetration in metals. International Journal of Impact Engineering, 25(8), p. 787−803.
[12] Q. Yang, L. Stainier, and M. Ortiz, 2006. A variational formulation of the coupled thermo-mechanical boundary-value problem for general dissipative solids. Journal of the Mechanics and Physics of Solids, 54(2), p. 401−424.
[13] B. Li, L. Perotti, M. Adams, J. Mihaly, L. Stainier, A. Jaramillo-Botero, A.J. Rosakis, M. Stalzer and Michael Ortiz, 2012. Optimal Transportation Meshfree (OTM) modeling of hypervelocity impact. (To be submitted)
[14] van Duin, A. C. T.; Dasgupta, S.; Lorant, F.; Goddard, W. A., 2001. ReaxFF:. A Reactive Force Field for Hydrocarbons. The Journal of Physical Chemistry A, 105 (41), p. 9396–9409.
[15] M. J. Assael, K. Kakosimos, R. M. Banish, J. Brillo, I. Egry, R. Brooks, P. N. Quested, K. C.Mills, A. Nagashima, Y. Sato, and W. A. Wakeham, 2006. Reference Data for the Density and Viscosity of Liquid Aluminum and Liquid Iron. Journal of Physical and Chemical Reference Data, 35(1), p. 285−300.
[16] J.M. Mihalya, A.J. Rosakisa, M.A. Adamsa, J.T. Tandya, 2012. Imaging Ejecta and Debris Cloud Behavior Using Laser Side-Lighting. The 12th Hypervelocity Impact Symposium.
[17] A. Pandolfi, B. Li, M. Ortiz, 2012. Modeling fracture within local max-ent meshfree approximation schemes. International Journal of Fracture. (Under Review)
[18] B. Li, A. Pandolfi, M.Ortiz, 2012. Dynamic Fragmentation in Ductile Materials via Optimal Transportation Meshfree Method. Journal of Computational Physics. (Under Review)